• Basic Research •

Vacuolar protein sorting 35 regulates retinal neurovascular function *via* astrocyte-mediated inflammatory response in a diabetic mouse model

Cheng Li[1], *Yuan-Rui Sun*[1], *Qiu-Mei Hu*[1], *Lin-Lin Luo*[1], *Xi Chen*[1], *Shu-Hong Zhou*[2], *Jie Xu*[1], *Xue Li*[1], *Wei Liu*[1]

[1]Department of Ophthalmology, Daping Hospital, Army Medical Center, Army Medical University, Chongqing 400042, China

[2]Department of Laboratory Animal Center, Daping Hospital, Army Medical Center, Army Medical University, Chongqing 400042, China

Co-first Authors: Cheng Li and Yuan-Rui Sun

Correspondence to: Wei Liu and Xue Li. Department of Ophthalmology, Daping Hospital, Army Medical Center, Army Medical University, Chongqing 400042, China. liuwei111@tmmu.edu.cn; lixue07@tmmu.edu.cn

Received: 2026-03-05 Accepted: 2026-05-07

Abstract

● **AIM:** To explore how vacuolar protein sorting 35 (VPS35) regulates astrocytic inflammation, impairs retinal endothelial function and drives early diabetic retinopathy (DR) neurovascular lesions in diabetic mouse model.

● **METHODS:** A streptozotocin (STZ)-induced C57BL/6J diabetic mouse model was established. Retinal tissues were collected from 0 to 12wk after successful induction of diabetes. Protein expression levels of VPS35, glial fibrillary acidic protein (GFAP), excitatory amino acid transporter 2 (EAAT2), leucine-rich repeat kinase 2 (LRRK2), and vascular endothelium-associated proteins were assessed by Western blotting (WB). The interaction between VPS35 and LRRK2 was verified by co-immunoprecipitation. Vascular leakage and astrocyte activation were evaluated by fundus fluorescein angiography and retinal flat-mount immunofluorescence staining. Primary astrocytes were cultured *in vitro* and subjected to high-glucose stimulation or VPS35 knockdown. Cell activation, expression of glutamate transport-associated proteins, and inflammatory cytokine expression were examined. Supernatant fluid from the primary astrocytes was applied to human umbilical vein endothelial cells (HUVECs) to assess cell migration, proliferation, and tube formation capacity. The expression of proteins related to the nuclear factor kappa-B (NF-κB) pathway was also evaluated.

● **RESULTS:** In diabetic mice, retinal VPS35 protein expression exhibited a progressive decline beginning at 4wk post-diabetes onset, whereas GFAP protein expression increased significantly. By 8wk, marked astrocyte activation was observed, accompanied by retinal microvascular leakage and a reduction in vascular area. *In vivo* and *in vitro* experiments further confirmed that under high-glucose conditions, retinal VPS35 and EAAT2 protein levels were markedly decreased, while GFAP and LRRK2 protein levels were significantly elevated. Co-immunoprecipitation verified the physical interaction between VPS35 and LRRK2 in astrocytes. Finally, *in vitro* experiments demonstrated that both high-glucose stimulation and VPS35 knockdown led to astrocyte activation, upregulation of inflammatory cytokine expression, downregulation of EAAT2 and AMPA receptor subunit GLUA2, and upregulation of LRRK2. Treatment of HUVECs with supernatant fluid from these astrocytes enhanced cell migration but significantly inhibited cell proliferation and tube formation. WB analysis revealed markedly increased levels of NF-κB and phosphorylated NF-κB in the treated HUVECs.

● **CONCLUSION:** During early DR in mice model, decreased retinal VPS35 protein expression induces astrocyte-mediated inflammatory responses and glutamate transport dysfunction. Through the interaction between VPS35 and LRRK2, paracrine inflammatory cytokines subsequently activate the NF-κB signaling pathway in vascular endothelial cells, leading to endothelial dysfunction and further driving DR-associated neurovascular injury. This study provides novel insights into the pathogenesis of DR and highlights the potential of VPS35 as a target for early intervention in DR.

● **KEYWORDS:** diabetic retinopathy; vacuolar protein sorting 35; leucine-rich repeat kinase 2; nuclear factor kappa-B; excitatory amino acid transporter 2; blood-retinal barrier; astrocytes; neurovascular unit; mice

DOI:10.18240/ijo.2026.08.05

Citation: Li C, Sun YR, Hu QM, Luo LL, Chen X, Zhou SH, Xu J, Li X, Liu W. Vacuolar protein sorting 35 regulates retinal neurovascular function *via* astrocyte-mediated inflammatory response in a diabetic mouse model. *Int J Ophthalmol* 2026;19(8):1470-1483

INTRODUCTION

Diabetic retinopathy (DR) is the most common ocular complication in diabetic patients and a leading cause of visual impairment among working-age populations worldwide[1-5]. To date, disruption of the blood-retinal barrier (BRB), characterized by retinal capillary dilation, leakage, pericyte apoptosis, and basement membrane thickening, has been regarded as the fundamental pathological alteration underlying DR[6-8]. However, an increasing body of research into the pathogenesis of DR has demonstrated that structural and functional changes in neurons and glial cells, such as increased apoptosis of retinal ganglion cells (RGCs) and astrocyte activation, occur prior to the onset of microvascular pathology. These findings indicate that DR is not solely a microvascular disease but rather a neurovascular disorder characterized by the coexistence neurodegenerationtion and microangiopathy[9-11]. The retinal neurovascular unit (NVU) is precisely assembled from neurons, glial cells, and vascular cells, collectively maintaining BRB homeostasis and microenvironmental equilibrium. Metabolic disturbances in DR can induce glial cell activation, leading to the release of inflammatory cytokines that trigger neuroinflammation and consequently disrupt NVU function. In turn, degenerating glial cells further exacerbate inflammation, creating a vicious cycle that ultimately drives neurodegenerative changes in DR[12-17].

Within the retina, astrocytes are confined to the nerve fiber layer and ganglion cell layer, which coincide precisely with the location of the inner retinal vasculature. Astrocytes ensheathe blood vessels and participate in the formation of the BRB. This histological distribution confers upon astrocytes a pronounced relevance to inner retinal vascular pathology. Astrocytes extend across the retinal surface to monitor hypoxic conditions within the inner retina. During the early stages of DR, high-glucose-induced hypoxia triggers astrocyte activation, resulting in the production of vascular endothelial growth factor (VEGF), interleukin-6 (IL-6), interleukin-1 beta (IL-1β), tumor necrosis factor-alpha (TNF-α), and other inflammatory cytokines that disrupt BRB metabolic balance[18]. Astrocytes also regulate the membrane localization and distribution of glucose transporters, preferentially delivering blood-derived glucose to neurons. Under high-glucose conditions, this mechanism is suppressed, thereby precipitating neuronal energy metabolic dysfunction[19]. Müller cells, the principal glial cells indigenous to the retina, maintain microenvironmental homeostasis *via* the glutamate-glutamine cycle[20]. Under high-glucose conditions, microglia undergo M1-type polarization, unleashing an inflammatory cytokine storm that, in concert with pro-angiogenic factors, aggravates BRB disruption and pathological neovascularization[21]. Studies have shown that astrocytic changes in DR precede those of Müller cells and microglia[22-23].

Vacuolar protein sorting 35 (VPS35) is a core component of the retromer complex, a retrograde vesicle trafficking machinery. Its primary function is to mediate the protein sorting and transport of transmembrane receptors from endosomes to the trans-Golgi network or back to the cell surface. VPS35 plays a pivotal role in the pathogenesis of central neurodegenerative disorders such as Parkinson's disease (PD) and Alzheimer's disease (AD)[24-26]. Studies have demonstrated that VPS35-deficient mice exhibit visual dysfunction, accompanied by Lewy body-like inclusions and phosphorylated α-synuclein aggregation in the retina, suggesting that VPS35 deficiency promotes the abnormal accumulation of α-synuclein within late endosomes[27]. Reduced VPS35 expression has also been observed in hippocampal neurons of the central nervous system across various diabetic animal models, a phenotype resembling the VPS35 deficits seen in AD patients[25,28-30]. Our research group has previously established that VPS35 is stably expressed in mouse RGCs. VPS35 insufficiency leads to RGC degeneration and optic nerve gliosis, manifested by reduced axonal and dendritic processes, thinning of the retinal nerve fiber layer, increased RGC apoptosis, and hyperphosphorylation of Tau protein in the retina[31-32]. Unpublished data from our group indicate that VPS35$^{+/m}$ mice exhibit enhanced retinal vascular leakage, and with advancing age, develop astrocytic structural disruption, increased RGC apoptosis, and a series of pathological features resembling those of DR. These phenotypes are consistent with early changes observed in DR[33]. We therefore employed a diabetic mouse model to conduct further investigations and found that retinal VPS35 expression progressively declines with the prolongation of the diabetic disease course. Moreover, high glucose markedly affects VPS35 expression in astrocytes. These observations suggest that VPS35 likely contributes to microvascular pathology by influencing retinal astrocytes. Consequently, the present study aims to elucidate the mechanistic role of VPS35 in regulating retinal vascular function *via* the modulation of astrocyte-mediated neuroinflammatory responses during the pathogenesis of DR.

MATERIALS AND METHODS

Ethical Approval The study protocol was approved by the Laboratory Animal Welfare and Ethics Committee of Army Medical University (No.AMUWEC20224779).

Streptozotocin-Induced Diabetic Mouse Model C57BL/6 wild-type mice (6–8 weeks old, body weight 20±2 g) were

purchased from the Animal Experimental Center of Army Medical Center and housed in the barrier facility of the same center. Male C57BL/6 mice aged 6–8wk were randomly divided into a control group and a diabetic model group using a random number table method (n=60 per group). Mice in the diabetic model group received daily intraperitoneal injections of streptozotocin (STZ; Bioss, D21012) at a dose of 55 mg/kg for five consecutive days. Three days after the final injection, random blood glucose levels were measured *via* tail vein sampling. Mice with a blood glucose level ≥16.7 mmol/L were considered successfully diabetic, yielding a modeling success rate of 86.7% (52/60). No mortality occurred in either the diabetic or control groups during the observation period.

Primary Astrocyte Culture and Identification Primary astrocytes were isolated and cultured according to previously described methods[34-35]. Immunofluorescence staining of the primary cultured astrocytes demonstrated that the percentage of glial fibrillary acidic protein (GFAP)-positive cells exceeded 95%, and the cells exhibited typical astrocytic morphology, confirming their suitability for subsequent experiments.

HUVECs Culture and Identification The human umbilical vein endothelial cells (HUVECs), HUVEC-T1 cell line (Cellcook, CC4004), was cultured in Dulbecco's modified eagle medium (DMEM) supplemented with 10% fetal bovine serum (FBS) and 1% penicillin-streptomycin at 37℃ in a 5% CO_2 incubator. Upon reaching 90% confluence, cells were passaged at a 1:3 ratio. Cells were cryopreserved in freezing medium at –80℃ overnight and subsequently stored in liquid nitrogen. Cells at passages 3–8 were used for all experiments. Immunofluorescence staining confirmed that the percentage of cluster of differentiation 31 (CD31) positive cells exceeded 95%, and the cells displayed a typical cobblestone-like morphology.

siRNA-Mediated VPS35 Knockdown in Astrocytes Primary astrocytes were seeded into 12-well plates. Upon reaching 40% confluence, cells were transfected with si-VPS35 or negative control siRNA (si-NC; RiboBio) according to the manufacturer's instructions for 24h. The medium was then replaced with DMEM containing 10% FBS, and cells were cultured until 90% confluence. Culture supernatant fluid and cellular protein were collected for subsequent analyses. The experiment included a si-NC group and three independent si-VPS35 sequence groups, with three replicate wells per group. Knockdown efficiency was verified by Western blotting (WB), and the most effective sequence was selected for subsequent experiments.

Western Blotting Retinal tissue or cells were lysed on ice for 30min in RIPA lysis buffer containing protease and phosphatase inhibitors. Lysates were centrifuged at 12 000 r/min for 15min at 4℃, and the supernatant was collected. Protein concentration was determined using a BCA assay kit, and samples were adjusted to equal concentrations. After adding 5×loading buffer, samples were denatured in a boiling water bath for 10min and stored at –20℃. Protein samples (10 μL) were separated on 10% SDS-PAGE gels by electrophoresis at 80 V until the marker bands were resolved, followed by 120 V until completion. Proteins were transferred to polyvinylidene fluoride membranes at a constant current of 250 mA for 90min. Membranes were blocked with 5% non-fat milk for 1.5h, incubated with primary antibodies overnight at 4℃, and then incubated with secondary antibodies for 1.5h at room temperature. Signals were detected using enhanced chemiluminescence.

Retinal Flat-Mount Preparation and IB4 Immunofluorescence Staining Mice were anesthetized by intraperitoneal injection of 1% sodium pentobarbital (50 mg/kg) and perfused with normal saline. Eyeballs were enucleated and fixed in cell fixation solution on ice for 1h. Retinas were dissected under a microscope, cut radially, and fixed in methanol for 30min. Retinas were transferred to 48-well plates, rinsed with normal saline, and blocked with goat serum containing 5% Triton X-100 overnight at 4℃. Primary antibody incubation was performed at 4℃ for 48h. After rinsing with normal saline, retinas were incubated with fluorophore-conjugated secondary antibody overnight at 4℃. Subsequently, retinas were incubated with isolectin B4 (IB4, Alexa Fluor 594, Invitrogen, I21413) overnight at 4℃. Following thorough rinsing, retinas were mounted with antifade mounting medium and imaged using a high-resolution microscope.

Cell Immunofluorescence Staining Primary astrocytes were seeded onto coverslips in 48-well plates. Upon reaching 40%–50% confluence, cells were divided into a control group and a high-glucose group (50 mmol/L) and treated for 48h, after which supernatant fluid was collected. Cells were washed with phosphate-buffered saline (PBS), fixed with fixation solution for 15min, permeabilized with 0.3% Triton X-100 for 10min, and blocked with 3% bovine calf serum for 1h. Cells were incubated with primary antibodies overnight at 4℃, followed by fluorophore-conjugated secondary antibodies for 1h at room temperature. Coverslips were mounted with DAPI-containing antifade mounting medium and imaged using a high-resolution microscope.

HUVEC Scratch Wound Healing Assay HUVECs were seeded into 12-well plates and cultured until 100% confluence. A vertical scratch was created in each well using a 10 μL pipette tip. After washing with PBS, cells were assigned to the following treatment groups: control group (DMEM complete medium), high-glucose group (50 mmol/L), normal astrocyte supernatant fluid group, high-glucose-stimulated

astrocyte supernatant fluid group, and lipopolysaccharide (LPS)-stimulated astrocyte supernatant fluid group. Images were captured at fixed positions at 0, 12, and 24h post-scratch. Scratch widths were measured using ImageJ software, and statistical analyses were performed.

HUVEC Proliferation Assay HUVECs were seeded onto coverslips in 48-well plates at a density of 5×10^4 cells per well. Upon reaching 30%–40% confluence, cells were assigned to the following groups and treated for 48h: control group, high-glucose group (50 mmol/L), normal astrocyte supernatant fluid group, high-glucose-stimulated astrocyte supernatant fluid group, and si-VPS35 astrocyte supernatant fluid group. 5-Ethynyl-2'-deoxyuridine (EdU) staining was performed using the EdU assay kit (RiboBio, C10310) according to the manufacturer's instructions. Images were acquired using a fluorescence microscope, and the percentage of EdU-positive cells was quantified.

HUVEC Tube Formation Assay A 48-well plate was pre-coated with Matrigel (200 μL per well), incubated at 4℃ for 10min, and then transferred to 37℃ for 30min to solidify. HUVECs were seeded at a density of 5×10^4 to 6×10^4 cells per well and assigned to the following groups: control group, high-glucose group (50 mmol/L), normal astrocyte supernatant fluid group, high-glucose-stimulated astrocyte supernatant fluid group, and si-VPS35 astrocyte supernatant fluid group. Tube formation was observed and photographed at 3, 6, and 8h. The number of junctions, number of branches, and total tube length were quantified using the ImageJ Angiogenesis Analyzer plugin.

Fundus Fluorescein Angiography Mice were anesthetized by intraperitoneal injection of 1% sodium pentobarbital (50 mg/kg), and pupils were dilated with compound tropicamide eye drops. Fluorescein sodium (0.5%, 10 mL/kg; Alcon) was administered *via* intraperitoneal injection. Fundus vascular imaging was performed immediately using a Heidelberg laser scanning ophthalmoscope.

Quantitative Real-Time Reverse Transcription Polymerase Chain Reaction Total RNA was extracted, and reverse transcription was performed to obtain complementary DNA (cDNA) according to the manufacturer's protocols. Quantitative real-time reverse transcription polymerase chain reaction (RT-qPCR) was carried out using the ChamQ Universal SYBR qPCR Master Mix kit (Vazyme, Q711-02/03) on a StepOnePlus RT-qPCR detection system (Thermo Fisher Scientific, USA). The thermal cycling conditions were as follows: initial denaturation at 95℃ for 3min, followed by 30 cycles of 95℃ for 15s and 55℃ for 30s. Relative gene expression levels were calculated using the $2^{-\Delta\Delta Ct}$ method.

Co-Immunoprecipitation of VPS35 and Leucine-Rich Repeat Kinase 2 Primary astrocytes were washed with PBS and lysed on ice for 20min in lysis buffer containing protease inhibitors at a ratio of 30 μL per 1×10^5 cells. Lysates were centrifuged at 12 000 r/min for 15min at 4℃, and the supernatant was collected. Magnetic beads were washed with PBST and subsequently incubated with anti-VPS35 or anti-leucine-rich repeat kinase 2 (LRRK2) primary antibody (30 μg/mL) at room temperature for 30min, followed by incubation at 4℃ for 2h. For the negative control group, species-matched immunoglobulin G was used in place of the primary antibody. After washing, the antibody-conjugated beads were incubated with the protein supernatant at room temperature for 30min and then at 4℃ for 2h. Following additional washes, 1×loading buffer was added, and the samples were heated at 95℃ for 5min. The eluted supernatant was then collected for WB analysis.

Statistical Analysis Statistical analyses were performed using GraphPad Prism 9.5 software. All continuous data were assessed for normality and homogeneity of variance. Data meeting the assumptions of normal distribution and equal variance were analyzed using parametric tests; otherwise, nonparametric tests were employed. Data are expressed as mean±standard error of the mean (SEM). Each experiment included at least three independent replicates. Comparisons between two groups were performed using Student's *t*-test. Comparisons among multiple groups were conducted using one-way or two-way analysis of variance (ANOVA), followed by Tukey's, Dunnett's, or Sidak's post hoc tests for pairwise comparisons, as appropriate. For correlation analyses, Pearson correlation analysis was applied when data conformed to a bivariate normal distribution; otherwise, Spearman rank correlation analysis was used. $P<0.05$ was considered statistically significant.

RESULTS

Early Retinal Microvascular Pathology in the Diabetic Mouse Model Fundus fluorescein angiography (FFA) revealed marked retinal microvascular leakage and structural disorganization in diabetic mice at 8wk post-STZ induction (Figure 1A, 1B). WB analysis demonstrated that retinal expression of CD31 and claudin-5 began to decline significantly at 4wk post-diabetes onset, with the most pronounced reductions observed at 8 and 10wk (Figure 1C–1E). Retinal flat-mount IB4 staining and Angio Tool quantitative analysis showed that from 8wk onward, diabetic mice exhibited decreased numbers of vascular junctions and total vessel area, increased mean vascular lacunarity, and visibly narrowed vessels, whereas no significant alterations in these parameters were detected at 0 or 4wk (Figure 1F–1I). Collectively, these findings demonstrate that STZ-induced diabetic mice develop unequivocal retinal microvascular injury by 8wk after successful induction of diabetes.

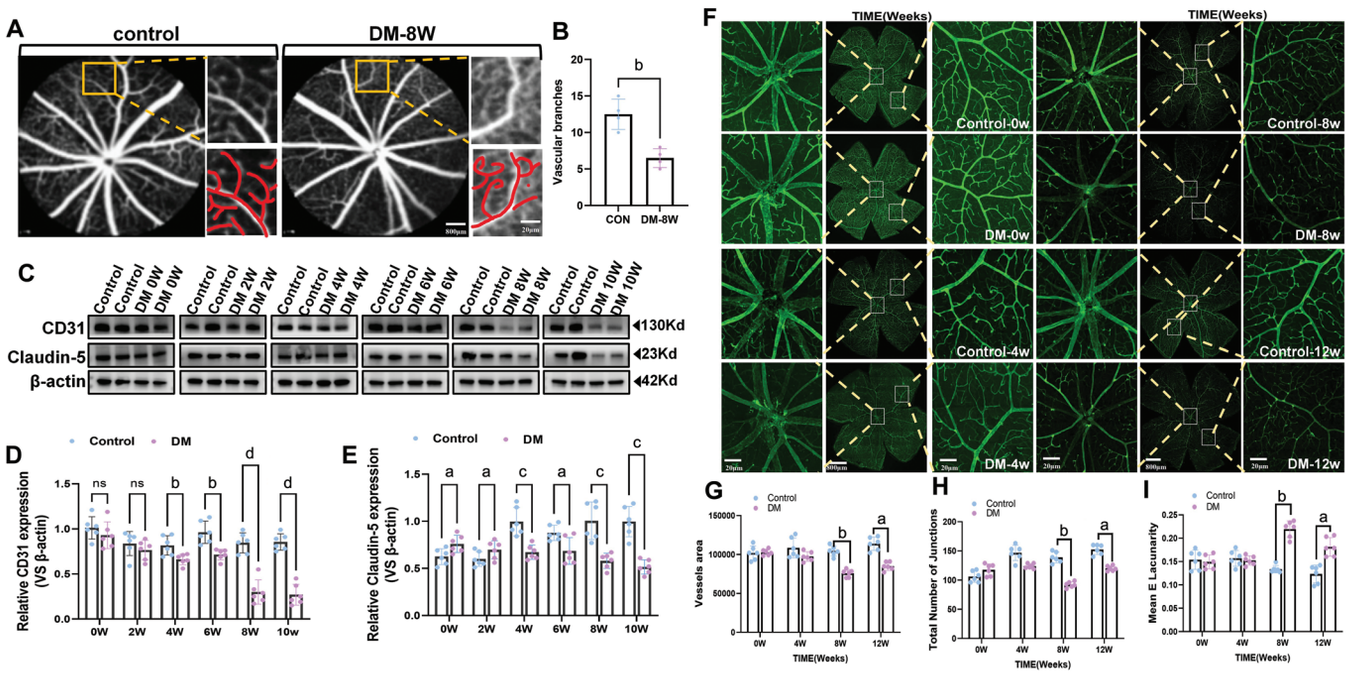

Figure 1 Retinal microvascular pathology in diabetic mice from 0 to 12wk post-diabetes onset A, B: Representative FFA images from CON and DM mice and quantification of vascular branch number. Data were analyzed using an unpaired *t*-test and are presented as mean±SEM; *n*=4. C–E: WB analysis of retinal CD31 and claudin-5 protein expression and corresponding quantitative analysis. Data were analyzed using an unpaired *t*-test and are presented as mean±SEM; *n*=6 per time point. F–I: IB4 staining of retinal flat-mounts and quantitative analysis of vascular parameters using Angio Tool software. Data were analyzed using an unpaired *t*-test and are presented as mean±SEM; *n*=6 per time point. [a]*P*<0.05, [b]*P*<0.01, [c]*P*<0.001, [d]*P*<0.0001 *vs* age-matched control group. CON: Control; DM: Diabetes mellitus; CD31: Cluster of differentiation 31; FFA: Fundus fluorescein angiography; IB4: Isolectin B4; SEM: Standard error of the mean.

Early Retinal Astrocyte Activation and Decreased VPS35 Expression in Diabetic Mouse Model In the retinal tissue of diabetic mice, compared with age-matched normal controls, VPS35 protein expression began to decline progressively from 4wk after successful induction of diabetes and decreased further with prolongation of the disease course. GFAP expression increased immediately upon successful diabetes induction and continued to rise as the disease progressed. S100 calcium-binding protein B (S100B) expression gradually increased from 4wk onward (Figure 2A–2D). These findings indicate that retinal astrocytes are activated during the early stages of diabetes. Retinal flat-mount preparations revealed that at 4wk post-diabetes onset, VPS35 fluorescence appeared more diffusely distributed, although the fluorescence intensity did not yet differ significantly from that of controls. By 8wk, however, VPS35 fluorescence intensity was markedly reduced compared with the normal control group (Figure 2E–2F). At the same time point (8wk), GFAP fluorescence intensity was significantly enhanced in the diabetic retina, and astrocytes exhibited thickened and shortened processes with reduced branching (Figure 2G–2H), further confirming astrocyte activation. Pearson correlation analysis demonstrated that retinal VPS35 protein expression in diabetic mice was negatively correlated with GFAP (r=–0.511, P=0.0039), positively correlated with CD31 (r=0.5068, P=0.0043), positively correlated with claudin-5 (r=0.3881, P=0.0341), and positively correlated with vascular area (r=0.7293, P=0.0006; Figure 2I–2L). These results suggest that VPS35 downregulation is closely associated with early neurovascular injury in diabetic retinopathy. In summary, decreased VPS35 expression and astrocyte activation may play important roles in early vascular injury during diabetic retinopathy.

High Glucose Reduces VPS35 Expression in Primary Astrocytes and Astrocyte-Derived Supernatant Fluid Promotes HUVEC Migration Primary astrocytes were treated with high glucose (50 mmol/L) for 1 to 3d. WB analysis revealed that VPS35 protein expression decreased progressively over time, whereas GFAP expression increased gradually. S100B and complement component 3 (C3) expression tended to decline, but the changes were not statistically significant (Figure 3A–3E). Immunofluorescence staining confirmed the cytoplasmic localization of VPS35 in astrocytes. In the high glucose group, VPS35 fluorescence intensity was markedly reduced, while GFAP fluorescence intensity was significantly enhanced (Figure 3F–3H).

Next, we collected supernatant fluid from primary astrocytes under normal control conditions, LPS stimulation, and high glucose treatment. These supernatant fluids were applied to cultured HUVECs, and a high-glucose directly treated HUVEC group was included for comparison. The scratch wound healing

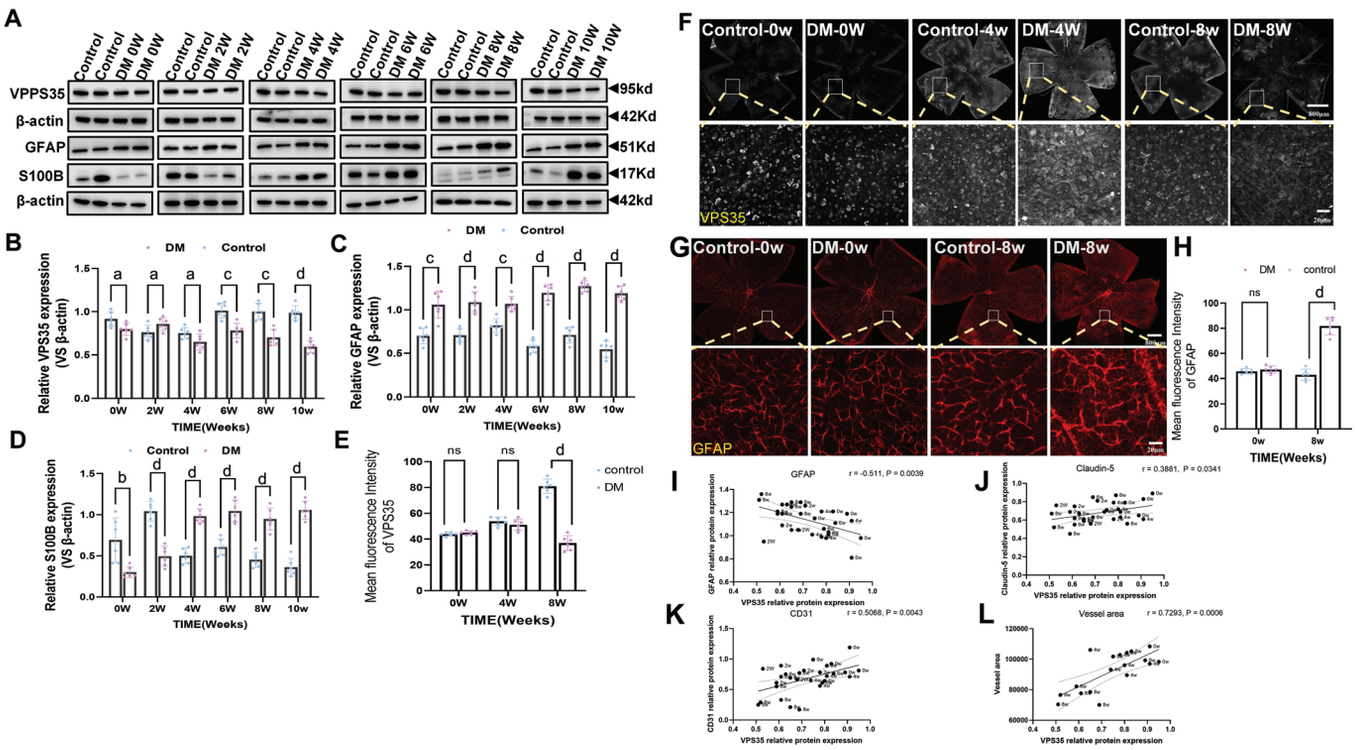

Figure 2 Temporal changes in retinal VPS35 and GFAP expression and correlation analysis in diabetic mice at different time points A: Representative WB bands of VPS35, GFAP, and S100B in the retina of CON and DM mice at 0, 2, 4, 6, 8, and 10wk post-diabetes onset. B–D: Quantification of VPS35, GFAP, and S100B protein levels. Data are presented as mean±SEM; *n*=6 per time point. Statistical analysis was performed using an unpaired *t*-test. E, F: Representative immunofluorescence images of VPS35 in retinal flat-mounts from CON and DM mice at different time points and corresponding quantitative analysis. G, H: Representative immunofluorescence images and quantification of GFAP in retinal flat-mounts from CON and DM mice at 0 and 8wk. Data are presented as mean±SEM; *n*=6 per time point, analyzed by unpaired *t*-test. I–L: Pearson correlation scatter plots between relative retinal VPS35 protein expression and GFAP, claudin-5, CD31, and vascular area (data from 0, 4, and 8wk) in diabetic mice. Solid lines represent linear regression, and shaded areas indicate 95% confidence bands. Each dot represents an individual diabetic mouse; *n*=36 (I–K) or *n*=18 (L). *r* is the Pearson correlation coefficient. $^{a}P<0.05$, $^{b}P<0.01$, $^{c}P<0.001$, $^{d}P<0.0001$ *vs* age-matched CON group. WB: Western blotting; VPS35: Vacuolar protein sorting 35; GFAP: Glial fibrillary acidic protein; S100B: S100 calcium-binding protein B; DM: Diabetes mellitus; CON: Control; SEM: Standard error of the mean; CD31: Cluster of differentiation 31.

assay was used to assess differences in HUVEC migration capacity among the groups. The results demonstrated that supernatant fluid from both LPS stimulated and high glucose treated astrocytes significantly promoted HUVEC migration, with the high glucose astrocyte supernatant fluid exhibiting the most potent pro-migratory effect. In contrast, direct high glucose treatment of HUVECs had no significant effect on their migration (Figure 3I–3K). These findings indicate that certain molecules secreted by astrocytes under high glucose conditions play a critical role in promoting HUVEC migration, rather than the high-glucose environment itself.

Supernatant Fluid from VPS35-Suppressed Astrocytes Induces HUVEC Dysfunction HUVECs were divided into five groups: normal control group, HG group, normal astrocyte supernatant fluid group, high-glucose-stimulated astrocyte supernatant fluid group, and si-VPS35-treated astrocyte supernatant fluid group. The EdU proliferation assay showed that the proliferative capacity of HUVECs in the high-glucose-stimulated astrocyte supernatant fluid group and the si-VPS35-treated astrocyte supernatant fluid group was lower than that in the control group, the high-glucose alone group, and the normal astrocyte supernatant fluid group (Figure 4A, 4B). The tube formation assay demonstrated that the number of junctions and the average tube length in the aforementioned two groups were lower than those in the other three groups (Figure 4C–4E). F-actin fluorescence staining revealed that in the normal control group, the HUVEC cytoskeleton exhibited an ordered arrangement of parallel stress fibers, whereas in the high-glucose-stimulated astrocyte supernatant fluid group and the si-VPS35 group, the mean fluorescence intensity was decreased, and the fibers were disorganized with reduced orientation; these alterations were more pronounced in the si-VPS35 group (Figure 4F–4H). WB analysis showed that protein expression of CD31 and claudin-5 in HUVECs was lower in the high-glucose-stimulated astrocyte supernatant fluid group and the si-VPS35 group

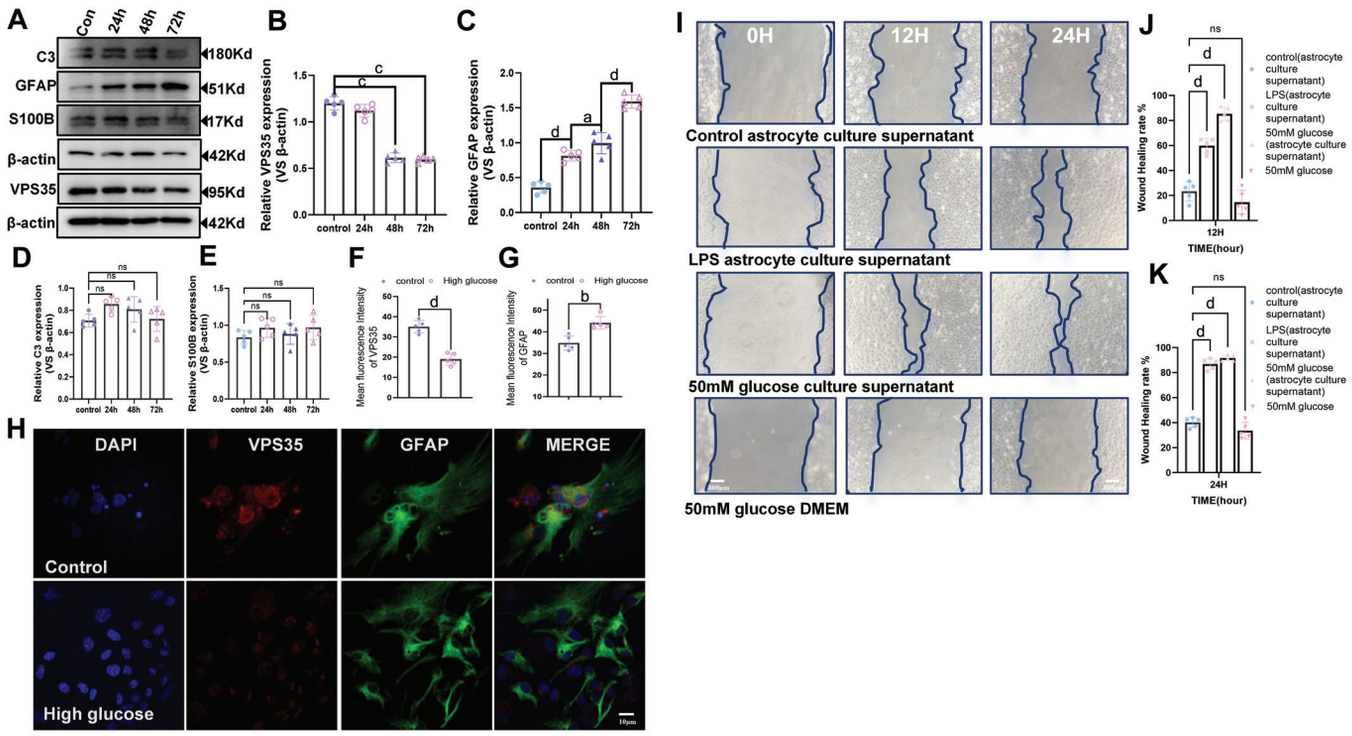

Figure 3 High glucose reduces VPS35 protein expression in primary astrocytes, and the effect of astrocyte-derived supernatant fluid on HUVEC migration A: Representative WB bands of VPS35, GFAP, S100B, C3 in primary astrocytes stimulated with high glucose (50 mmol/L) for 1, 2, and 3d. B–E: Quantification of VPS35, GFAP, C3, and S100B protein levels. Data are presented as mean±SEM; *n*=6. Statistical analysis was performed using an unpaired *t*-test. F–H: Representative immunofluorescence images of VPS35 (red) and GFAP (green) in primary astrocytes after 3d of high glucose stimulation, and quantification of fluorescence intensity. Data are presented as mean±SEM; *n*=6, analyzed by unpaired *t*-test. I: Representative images from the scratch wound healing assay at 0, 12, and 24h after treatment of HUVECs with the indicated conditioned media. Groups: control, high glucose, normal astrocyte supernatant fluid, high-glucose-stimulated astrocyte supernatant fluid, and LPS-stimulated astrocyte supernatant fluid. J, K: Quantification of wound healing rates at 12 and 24h. Data are presented as mean±SEM; *n*=6, analyzed by one-way ANOVA followed by Dunnett's multiple comparisons test. [a]*P*<0.05, [b]*P*<0.01, [c]*P*<0.001, [d]*P*<0.0001 *vs* control group. HUVEC: Human umbilical vein endothelial cell; VPS35: Vacuolar protein sorting 35; GFAP: Glial fibrillary acidic protein; S100B: S100 calcium-binding protein B; C3: Complement component 3; LPS: Lipopolysaccharide; SEM: Standard error of the mean; WB: Western blotting; ANOVA: Analysis of variance.

than in the other three groups, whereas glucose transporter 1 (GLUT1) protein expression was higher in these two groups than in the other three groups (Figure 4I–4L). Collectively, these results indicate that inhibition of VPS35 expression in astrocytes affects glucose transport function, leads to cytoskeletal disorganization in HUVECs, and suppresses their tube formation and proliferation.

Suppression of VPS35 in Astrocytes Promotes LRRK2 Expression, Inhibits EAAT2/GLUA2 Expression, and Enhances Inflammatory Cytokine Secretion Following high-glucose (50 mmol/L) treatment of primary astrocytes for 24, 48, and 72h, WB analysis revealed no significant change in excitatory amino acid transporter 1 protein expression, whereas excitatory amino acid transporter 2 (EAAT2) and glutamate receptor 2 (GLUA2) protein expression were downregulated, and LRRK2 protein expression was upregulated (Figure 5A, 5B). At 8wk after successful diabetes induction, retinal protein expression of VPS35, EAAT2, and GLUA2 was lower in diabetic mice than in control mice, whereas GFAP and LRRK2 protein expression was higher than in controls (Figure 5C, 5D). Following transfection of primary astrocytes with si-VPS35, GFAP and LRRK2 protein expression increased, while EAAT2 and GLUA2 protein expression decreased (Figure 5E, 5F). Co-immunoprecipitation (Co-IP) analysis demonstrated an interaction between VPS35 and LRRK2 in primary astrocytes (Figure 5G). RT-qPCR showed that under high-glucose treatment or si-VPS35 transfection, the mRNA expression of IL-1β, IL-6, and TNF-α in primary astrocytes was higher than that in the control group (Figure 5H–5J). These results indicate that under high-glucose conditions, reduced VPS35 expression in retinal astrocytes leads to astrocyte activation and disruption of glutamate homeostasis *via* upregulation of LRRK2 expression, thereby promoting the secretion of inflammatory cytokines.

Supernatant Fluid from VPS35-Knockdown Astrocytes Activates NF-κB and Suppresses FoxM1/HIF-1α in HUVECs Following treatment of HUVECs with supernatant fluid from si-VPS35-treated astrocytes, WB analysis revealed

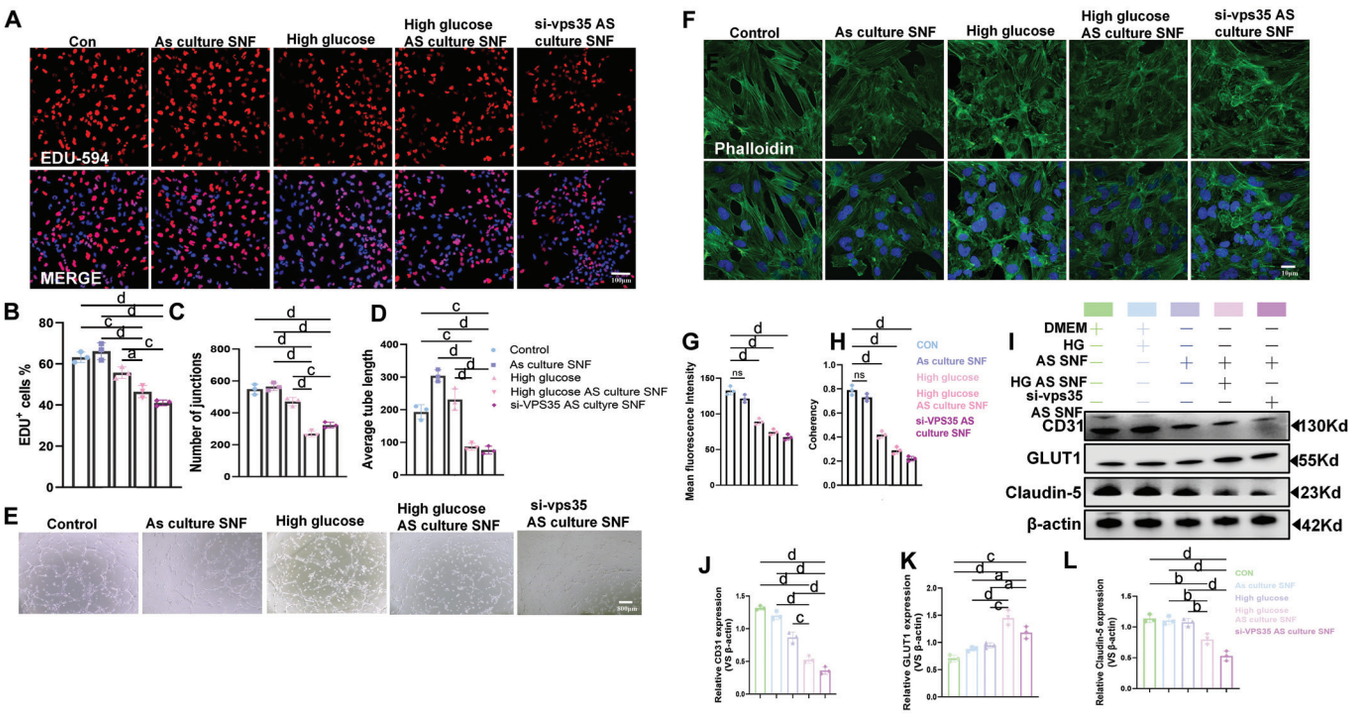

Figure 4 Effects of supernatant fluid from primary astrocytes under different treatment conditions on HUVEC proliferation, morphology, and protein expression of CD31, claudin-5, and GLUT1 A, B: EdU assay showing the effect of supernatant fluid from primary astrocytes under different treatment conditions on HUVEC proliferation, with corresponding statistical analysis. C–E: Effects of supernatant fluid from primary astrocytes under different treatment conditions on the number of junctions and average tube length in the HUVEC tube formation assay, with statistical analysis. F–H: F-actin fluorescence staining showing the effect of supernatant fluid from primary astrocytes under different treatment conditions on the mean fluorescence intensity and fiber organization of the HUVEC cytoskeleton, with statistical analysis. I–L: WB analysis of CD31, claudin-5, and GLUT1 protein expression in HUVECs treated with supernatant fluid from the following groups: normal control, high-glucose alone, normal astrocyte supernatant fluid, high-glucose-stimulated astrocyte supernatant fluid, and si-VPS35-treated astrocyte supernatant fluid, with corresponding statistical analysis. Data are presented as mean±SEM; n=3. Statistical analysis was performed using one-way ANOVA followed by Tukey's post hoc test. ^{a}P<0.05, ^{b}P<0.01, ^{c}P<0.001, ^{d}P<0.0001. HUVECs: Human umbilical vein endothelial cells; HG: High glucose; AS SNF: Astrocyte culture supernatant fluid; HG AS SNF: High glucose-stimulated astrocyte culture supernatant fluid; si-VPS35 AS SNF: si-VPS35-treated astrocyte culture supernatant fluid; CD31: Cluster of differentiation 31; GLUT1: Glucose transporter 1; WB: Western blotting; SEM: Standard error of the mean; EdU: 5-Ethynyl-2'-deoxyuridine; ANOVA: Analysis of variance.

that protein expression of nuclear factor kappa-B (NF-κB) and phosphorylated NF-κB (p-NF-κB) increased from day 2 onward, whereas protein expression of hypoxia-inducible factor 1-alpha (HIF-1α) and forkhead box protein M1 (FoxM1) decreased (Figure 6). These results indicate that following VPS35 reduction in astrocytes, the derived supernatant fluid activates the NF-κB inflammatory pathway in adjacent vascular endothelial cells.

DISCUSSION

Disruption of the BRB and the resultant retinal microangiopathy have long been regarded as the fundamental pathological alterations in DR. In recent years, however, techniques such as neuroelectrophysiology, optical coherence tomography, and microperimetry have revealed that abnormalities in the electroretinogram, foveal thickness, and mean retinal sensitivity of the central fovea are already present in diabetic patients even in the absence of clinically evident retinal microvascular lesions[9,36-38]. Accumulating evidence indicates that DR is a neurovascular disorder characterized by the coexistence of neurodegeneration and microangiopathy, and that structural and functional alterations in neurons and glial cells precede the onset of microvascular pathology[9,33,37-39]. These findings suggest that pathological changes in neural cells and microvascular injury may occur concurrently in the diabetic state, and that DR is not solely a microvascular disease but rather a neurovascular disorder comprising both neurodegenerative and microvascular components. Moreover, an increasing body of research has confirmed that the NVU plays a pivotal role in DR. The literature indicates that metabolic disturbances in DR lead to reciprocal interactions among the various constituents of the NVU, such that dysfunction of any single component can precipitate overall NVU impairment. Specifically, a series of metabolic abnormalities in DR activate retinal glial cells, which in turn produce a variety of

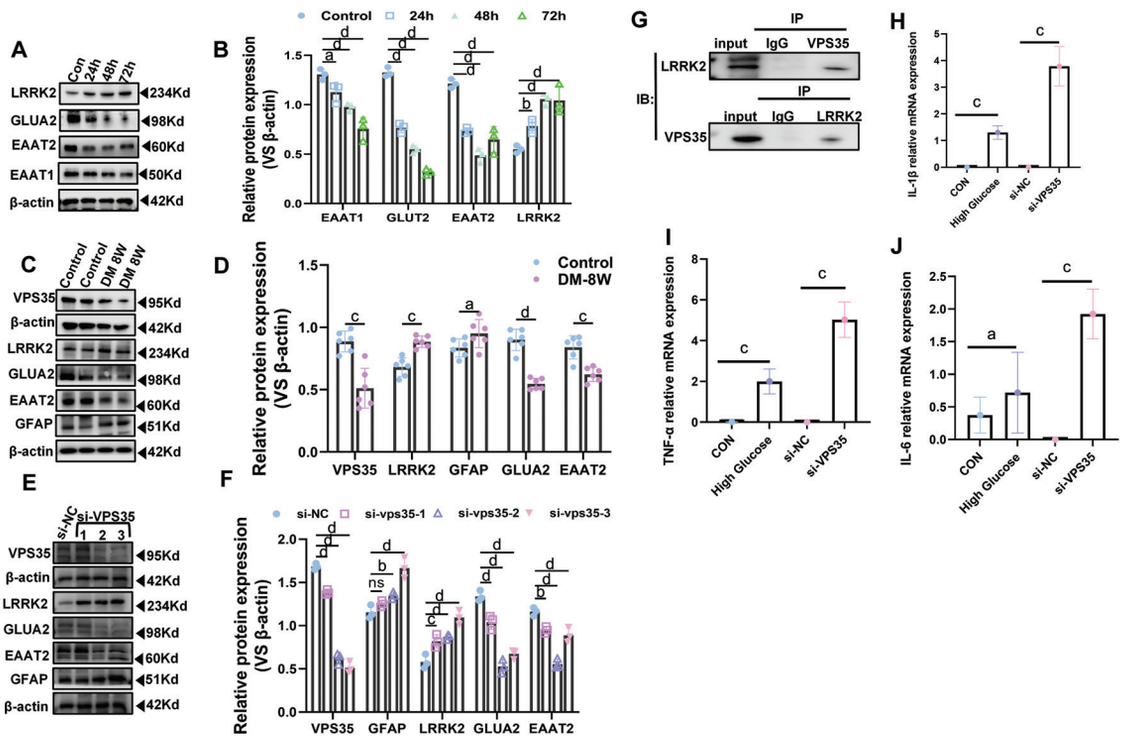

Figure 5 Effects of VPS35 knockdown in primary astrocytes on LRRK2, EAAT2, and GLUA2 protein expression and proinflammatory cytokine mRNA levels, and the interaction between VPS35 and LRRK2 A, B: WB analysis of EAAT1, excitatory EAAT2, LRRK2, and GLUA2 protein expression in primary astrocytes under high-glucose stimulation at different time points, with corresponding quantitative analysis. Data are presented as mean±SEM; *n*=3. Statistical analysis was performed using two-way ANOVA followed by Sidak's post hoc test. C, D: WB analysis of VPS35, GFAP, EAAT2, GLUA2, and LRRK2 protein expression in the retina at 8wk post-diabetes onset, with quantitative analysis. Data are presented as mean±SEM; *n*=6, analyzed by *t*-test. E, F: WB analysis of EAAT2, GFAP, GLUA2, and LRRK2 protein expression in primary astrocytes after VPS35 knockdown, with quantitative analysis. Data are presented as mean±SEM; *n*=3, analyzed by two-way ANOVA followed by Sidak's post hoc test. G: Co-IP assay showing the interaction between VPS35 and LRRK2. H–J: RT-qPCR analysis of the relative mRNA expression levels of IL-1β, TNF-α, and IL-6 in primary astrocytes under normal control, high-glucose treatment, si-NC, and si-VPS35 knockdown conditions. Data were normalized to β-actin and are presented as mean±SEM; *n*=3 independent experiments. Statistical analysis was performed using one-way ANOVA followed by Tukey's post hoc test. [a]*P*<0.05, [b]*P*<0.01, [c]*P*<0.001, [d]*P*<0.0001. LRRK2: Leucine-rich repeat kinase 2; GLUA2: Glutamate receptor 2; EAAT2: Excitatory amino acid transporter 2; EAAT1: Excitatory amino acid transporter 1; AS: Astrocyte; SNF: Supernatant fluid; IL-1β: Interleukin-1 beta; IL-6: Interleukin-6; TNF-α: Tumor necrosis factor-alpha; RT-qPCR: Quantitative real-time reverse transcription polymerase chain reaction; Co-IP: Co-immunoprecipitation; WB: Western blotting; SEM: Standard error of the mean; VPS35: Vacuolar protein sorting 35; GFAP: Glial fibrillary acidic protein; CON: Control; DM: Diabetes mellitus; ANOVA: Analysis of variance.

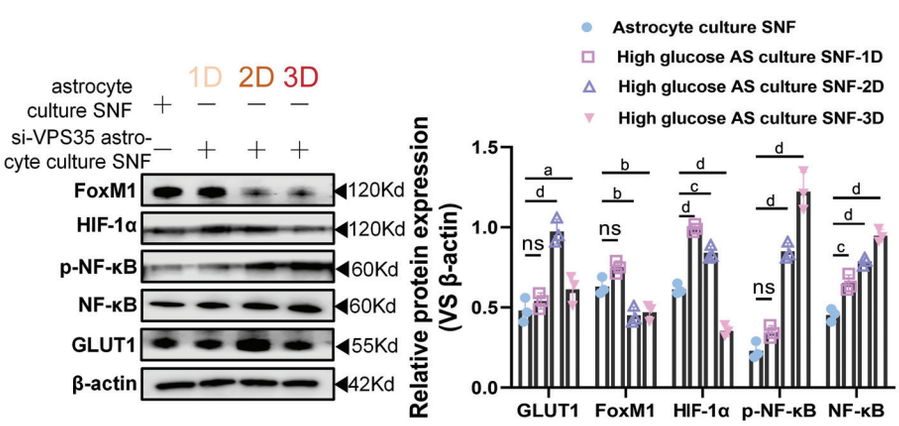

Figure 6 Knockdown of VPS35 in astrocytes activates the NF-κB signaling pathway in HUVECs WB analysis of HIF-1α, FoxM1, NF-κB, and p-NF-κB protein expression in HUVECs treated with supernatant fluid from si-VPS35-treated astrocytes at different time points, with corresponding statistical analysis. Data are presented as mean±SEM; *n*=3 independent experiments. Statistical analysis was performed using two-way ANOVA followed by Sidak's post hoc test. [a]*P*<0.05, [b]*P*<0.01, [c]*P*<0.001, [d]*P*<0.0001. HIF-1α: hypoxia-inducible factor 1-alpha; FoxM1: Forkhead box protein M1; NF-κB: Nuclear factor kappa-B; p-NF-κB: Phosphorylated nuclear factor kappa-B; SNF: Supernatant fluid; WB: Western blotting; SEM: Standard error of the mean; VPS35: Vacuolar protein sorting 35; HUVECs: Human umbilical vein endothelial cells; SNF: Supernatant fluid; GLUT1: Glucose transporter 1; ANOVA: Analysis of variance.

inflammatory cytokines, chemokines, and growth factors. These mediators incite retinal neuroinflammation, thereby compromising NVU function. Degenerating glial cells further exacerbate the neuroinflammatory response, creating a vicious cycle that progressively drives neurodegenerative changes in DR[12-17].

Astrocytes in the retina exhibit two distinct morphological phenotypes and tissue localizations, which are classified as either neurotoxic (A1) or neuroprotective (A2)[40-41]. A1 astrocytes are characterized by high expression of complement components (*e.g.,* C3), S100B, and proinflammatory cytokines, whereas A2 astrocytes highly express neurotrophic factors such as S100 calcium-binding protein A10[42]. Our study demonstrated elevated S100B expression in the diabetic mouse model, indicative of astrocyte activation and the consequent exertion of neurotoxic effects. Studies have shown that astrocytic changes in DR precede those of Müller cells and microglia[22-23]. Previous research has confirmed that during the development and progression of DR, astrocyte activation triggered by high-glucose-induced hypoxia can be detected at the earliest stages of the disease. Activated astrocytes produce inflammatory factors such as VEGF, IL-6, IL-1β, thereby initiating a neuroinflammatory cascade that ultimately disrupts BRB homeostasis. Moreover, activated astrocytes release chemokines that recruit and activate microglia, further amplifying the inflammatory response and accelerating neurovascular pathology[18]. Consistent with these findings, studies employing STZ-induced diabetic animal models have demonstrated that the earliest neurodegenerative alterations occur along the visual pathway, with disease progression leading to retinal vascular damage, and astrocyte activation represents the most prominent early change in this process[43-44]. Our own findings revealed that in the retinas of diabetic mice at early disease stages, GFAP expression began to increase significantly at week 0 and progressively migrated from the ganglion cell layer toward the inner plexiform layer by week 12, suggesting that astrocyte activation commences early following high-glucose exposure. In contrast, immunofluorescence labeling of Müller cells with vimentin indicated that their activation occurred at week 10. considerably later than that of astrocytes.

VPS35, a core component of the retromer complex, is well established to be intimately associated with central neurodegenerative disorders such as AD and PD. Our research group previously demonstrated that VPS35 heterozygous knockout mice ($VPS35^{+/m}$) exhibit impaired RGC axons and thinning of the retinal nerve fiber layer[31], as well as phenotypes characteristic of DR, including enhanced retinal vascular leakage, disrupted astrocyte architecture, and increased RGC apoptosis. Together with literature reports of a marked deficiency of VPS35 in the hippocampal tissue of diabetic mouse models, these findings strongly suggest that VPS35 may represent a convergent point in the shared pathogenesis of AD and diabetes[30]. In the present study, we further found that retinal VPS35 expression progressively declines in diabetic mice beginning at 4wk post-diabetes onset, concomitant with astrocyte activation that is initiated at the very early stage of diabetes and becomes progressively enhanced as the disease advances. Subsequent cell-based experiments confirmed that high-glucose stimulation of primary astrocytes leads to astrocyte activation and a significant reduction in cytoplasmic VPS35 expression compared with the normal control group. Collectively, these results demonstrate that retinal astrocytes are activated during early diabetes in parallel with a decrease in VPS35 expression, and Pearson correlation analysis confirmed a significant association between these two events. We therefore speculate that the reduction of VPS35 under high-glucose conditions may be a causative factor in astrocyte activation.

Studies have demonstrated that, in addition to its role in neurodegeneration, VPS35 dysfunction plays a critical role in vascular differentiation and maturation during mouse brain development. VPS35 deficiency markedly increases the activity of reactive astrocytes associated with vascular differentiation and maturation, thereby accelerating vascular endothelial cell apoptosis[29,45-46]. The present study found that inhibition of VPS35 expression in primary astrocytes leads to cytoskeletal disorganization in vascular endothelial cells, decreased tube formation capacity, impaired cell proliferation, and concomitant abnormalities in glucose transport function. These findings indicate that VPS35 exerts a key regulatory role in the interaction between astrocytes and vascular endothelial cells under high-glucose conditions. LRRK2 represents the most common cause of autosomal dominant PD and is associated with abnormal vesicle trafficking, leading to shortened neuronal axons and dendrites, thereby playing a significant role in neurodegenerative diseases[47-48]. Literature reports indicate that LRRK2 is highly expressed in the brain tissue of diabetic rat models, and that VPS35 can induce disease progression through activation of LRRK2, although the precise underlying mechanism remains unclear[49-51]. Using Co-IP assays in primary astrocytes, we confirmed an interaction between VPS35 and LRRK2 in astrocytes, which is consistent with previous reports demonstrating their spatial and functional interaction in brain tissue[52]. Furthermore, our study demonstrated that LRRK2 expression is significantly upregulated both in the retinal tissue of diabetic mice and in astrocytes activated by high glucose. Moreover, cell-based experiments revealed that knockdown of VPS35 in astrocytes leads to astrocyte activation accompanied by a marked

increase in LRRK2 expression. These results suggest that under high-glucose conditions, VPS35 may function as a negative regulator of LRRK2. Decreased VPS35 expression disrupts normal protein sorting homeostasis, resulting in abnormal accumulation or enhanced kinase activity of LRRK2 in astrocytes, thereby triggering astrocyte activation.

Glutamate (Glu) is the most abundant, widely distributed, and potent excitatory neurotransmitter in the central nervous system. Its excitotoxicity can cause various forms of neural injury and neurodegeneration. In the retina, Glu is extensively distributed across photoreceptors, bipolar cells, and the ganglion cell layer, where it plays a critical role in signal transmission. The rapid clearance of excess extracellular Glu is essential for maintaining normal retinal physiological function, and one of the functions of astrocytes is to participate in this clearance process. EAAT2 is the principal transporter responsible for Glu clearance in the central nervous system. Impairment of its function leads to synaptic Glu accumulation, resulting in neuronal excitotoxicity[53], and can also trigger reactive astrogliosis and further neurodegeneration[54-55]. Studies in brain tissue have shown that LRRK2 interferes with EAAT2 function, leading to extracellular Glu overload and consequent neurodegenerative changes[56-57]. GLUA2 is responsible for receiving Glu signals; its reduction exacerbates excitotoxic injury[58]. Thus, GLUA2 mediates Glu signal reception, while EAAT2 is responsible for Glu clearance, and together they maintain normal glutamatergic signaling while preventing excitotoxicity. Our study found that EAAT2 and GLUA2 expression levels were significantly reduced in both the retinal tissue of diabetic mice and in astrocytes subjected to high-glucose stimulation compared with normal controls. Furthermore, knockdown of VPS35 in astrocytes also markedly decreased EAAT2 and GLUA2 expression. These findings indicate that the specific downregulation of EAAT2 and GLUA2 signifies a disruption of synaptic Glu homeostasis in the retina. This series of changes suggests that aberrant VPS35-LRRK2 axis activity under high-glucose conditions may represent a critical upstream event leading to retinal Glu excitotoxicity and accelerated ganglion cell injury.

Astrocytes play a pivotal role within the retinal neurovascular unit, serving not only as supportive cells for neurons but also as guardians of the BRB. Our study demonstrates that upon VPS35 knockdown, astrocytes become activated and exhibit elevated expression of IL-1β, IL-6, and TNF-α. Treatment of vascular endothelial cells with supernatant fluid derived from these astrocytes results in a marked increase in NF-κB and p-NF-κB protein levels, accompanied by a significant decrease in HIF-1α and FoxM1 protein expression. NF-κB is a well-established master transcription factor that governs vascular permeability, leukocyte adhesion, and inflammatory responses. Previous studies have convincingly demonstrated that TNF-α disrupts the tight junction complex of retinal endothelial cells *via* activation of the NF-κB signaling pathway, leading to increased barrier permeability[59]. Moreover, NF-κB expression is known to escalate with the progression of diabetes and has been closely linked to retinal cell apoptosis and neovascularization[60]. Our findings reveal that under high-glucose conditions, astrocytes release multiple proinflammatory cytokines (TNF-α, IL-1β, IL-6), concomitant with a significant increase in NF-κB and p-NF-κB protein expression. This suggests that astrocytes likely contribute to the disruption of the BRB by activating the NF-κB pathway in vascular endothelial cells[61].

We therefore infer that reduced VPS35 expression in astrocytes under high-glucose conditions may activate the NF-κB pathway in vascular endothelial cells *via* a paracrine mechanism, thereby affecting endothelial cell function, although the precise underlying mechanisms warrant further in-depth investigation. Our study partially elucidates the mechanism by which VPS35 influences vascular endothelial function through astrocytes during the early stages of diabetes. However, certain limitations remain. Specifically, our mechanistic exploration relies predominantly on in vitro cell-based experiments. Future studies will necessitate the establishment of *in vivo* models, such as astrocyte-specific VPS35 knockout mice or VPS35-overexpressing mouse lines, to provide more direct validation and further investigation within a physiological context.

Current clinical treatments for DR primarily target the advanced neovascular stage, with anti-VEGF agents as the mainstay, whereas interventions addressing early neurodegenerative changes and vascular dysfunction remain relatively limited[62-63]. Our findings indicate that the VPS35-LRRK2-NF-κB signaling axis plays a significant role in neurovascular pathology during the early stages of DR, thereby providing a potential novel target for early intervention. Literature reports have shown that small-molecule compounds targeting the VPS35-LRRK2 interaction have demonstrated therapeutic potential in PD models, and several LRRK2 kinase inhibitors have entered clinical trial phases[64-66]. Consequently, this study suggests that, following further mechanistic exploration coupled with *in vivo* experimental validation, such VPS35-LRRK2-targeting small molecules might also be applicable for early intervention in DR, although their safety and efficacy require further investigation in diabetic animal models. Furthermore, our results underscore the driving role of astrocyte activation in DR-associated vascular endothelial dysfunction, implying that strategies aimed at modulating astrocyte activation, such as inhibiting LRRK2 kinase activity or enhancing VPS35 expression, may confer dual benefits of

neuroprotection and vascular stabilization. Considering recent advances in the regulation of Müller cell ferroptosis[67] and the inhibition of the stimulator of interferon genes pathway in microglia[68], future therapeutic strategies for DR may involve synergistic interventions targeting multiple glial cell types to achieve optimal treatment outcomes.

In conclusion, during early diabetic retinopathy, VPS35 mediates astrocyte inflammatory responses through the regulation of LRRK2, which activates the NF-κB signaling pathway. This activation leads to functional abnormalities in vascular endothelial cells, including impaired cytoskeletal stability, altered migration, and reduced proliferative capacity, thereby further driving retinal neurovascular dysfunction.

ACKNOWLEDGEMENTS

Authors' Contributions: Liu W, Li X, and Li C conceived the study. Li X, Li C, Sun YR, and Hu QM performed the cell experiments of this study. Li C, Sun YR, Luo LL, Li X, and Xu J performed the animal experiments in this study. Li X, Li C, Chen X, and Sun YR collected and organized the experimental data. Li X, Li C, and Sun YR performed the statistical analyses. Zhou SH carried out animal breeding and the establishment of animal models. Li X and Li C wrote the manuscript, and Liu W revised the manuscript critically. All authors approved the final version. Liu W is the guarantor of this work and, as such, had full access to all the data in the study and takes responsibility for the integrity of the data and the accuracy of the data analysis.

Availability of Data and Materials: All data generated or analyzed during this study are included in this published article and its supplementary information files can be requested from the corresponding author upon reasonable request.

Artificial Intelligence Statement Disclosure: The authors declare that no generative AI or AI-assisted technologies were used in the preparation or writing of this manuscript. All content was produced entirely by the authors without any automated assistance.

Foundations: Supported by the Natural Science Foundation of Chongqing, China (No.cstc2021jcyj-msxmX0164; No.CSTB2023NSCQ-MSX0593).

Conflicts of Interest: Li C, None; **Sun YR,** None; **Hu QM,** None; **Luo LL,** None; **Chen X,** None; **Zhou SH,** None; **Xu J,** None; **Li X,** None; **Liu W,** None.

REFERENCES

1 Li H, Liu X, Zhong H, *et al*. Research progress on the pathogenesis of diabetic retinopathy. *BMC Ophthalmol* 2023;23(1):372.

2 Su Z, Wu Z, Liang X, *et al*. Diabetic retinopathy risk in patients with unhealthy lifestyle: a Mendelian randomization study. *Front Endocrinol (Lausanne)* 2022;13:1087965.

3 Hou X, Wang L, Zhu D, *et al*. Prevalence of diabetic retinopathy and vision-threatening diabetic retinopathy in adults with diabetes in China. *Nat Commun* 2023;14:4296.

4 Sivaprasad S, Wong TY, Gardner TW, *et al*. Diabetic retinal disease. *Nat Rev Dis Primers* 2025;11:62.

5 Rai BB, Maddess T, Nolan CJ. Functional diabetic retinopathy: a new concept to improve management of diabetic retinal diseases. *Surv Ophthalmol* 2025;70(2):232-240.

6 Xu GT, Zhang JF, Tang L. Inflammation in diabetic retinopathy: possible roles in pathogenesis and potential implications for therapy. *Neural Regen Res* 2023;18(5):976.

7 Altmann C, Schmidt MHH. The role of microglia in diabetic retinopathy: inflammation, microvasculature defects and neurodegeneration. *Int J Mol Sci* 2018;19(1):110.

8 Yang X, Huang Z, Xu M, *et al*. Autophagy in the retinal neurovascular unit: New perspectives into diabetic retinopathy. *J Diabetes* 2023;15(5):382-396.

9 Shin YI, Nam KY, Lee SE, *et al*. Peripapillary microvasculature in patients with diabetes mellitus: an optical coherence tomography angiography study. *Sci Rep* 2019;9:15814.

10 Leal EC, Martins J, Voabil P, *et al*. Calcium dobesilate inhibits the alterations in tight junction proteins and leukocyte adhesion to retinal endothelial cells induced by diabetes. *Diabetes* 2010;59(10):2637-2645.

11 Heng LZ, Comyn O, Peto T, *et al*. Diabetic retinopathy: pathogenesis, clinical grading, management and future developments. *Diabet Med* 2013;30(6):640-650.

12 Nian S, Lo ACY, Mi Y, *et al*. Neurovascular unit in diabetic retinopathy: pathophysiological roles and potential therapeutical targets. *Eye Vis (Lond)* 2021;8(1):15.

13 Gardner TW, Bek T. Dissecting the neurovascular unit in human diabetic retinal disease. *Diabetes* 2024;73(11):1791-1792.

14 Grimes WN, Berson DM, Sabnis A, *et al*. Layer-specific anatomical and physiological features of the retina's neurovascular unit. *Curr Biol* 2025;35(1):109-120.e4.

15 Zhu H, Li B, Huang T, *et al*. Update in the molecular mechanism and biomarkers of diabetic retinopathy. *Biochim Biophys Acta BBA Mol Basis Dis* 2025;1871(5):167758.

16 Callan A, Jha S, Valdez L, *et al*. Cellular and molecular mechanisms of neuronal degeneration in early-stage diabetic retinopathy. *Curr Vasc Pharmacol* 2024;22(5):301-315.

17 Dharmarajan S, Carrillo C, Qi Z, *et al*. Retinal inflammation in murine models of type 1 and type 2 diabetes with diabetic retinopathy. *Diabetologia* 2023;66(11):2170-2185.

18 Vecino E, Rodriguez FD, Ruzafa N, *et al*. Glia–neuron interactions in the mammalian retina. *Prog Retin Eye Res* 2016;51:1-40.

19 Ardanaz CG, de la Cruz A, Minhas PS, *et al*. Astrocytic GLUT1 reduction paradoxically improves central and peripheral glucose homeostasis. *Sci Adv* 2024;10(42):eadp1115.

20 Biswas S, Shahriar S, Bachay G, *et al*. Glutamatergic neuronal activity regulates angiogenesis and blood-retinal barrier maturation *via* Norrin/β-catenin signaling. *Neuron* 2024;112(12):1978-1996.e6.

21 Bai Y, Wang X, Qi F, *et al*. Mechanisms of action of retinal microglia in diabetic retinopathy. *Int J Mol Med* 2025;56(6):202.

22 Paisley CE, Kay JN. Seeing stars: Development and function of retinal astrocytes. *Dev Biol* 2021;478:144-154.

23 Yoo HS, Shanmugalingam U, Smith PD. Harnessing astrocytes and Müller glial cells in the retina for survival and regeneration of retinal ganglion cells. *Cells* 2021;10(6):1339.

24 Cui Y, Yang Z, Teasdale RD. The functional roles of retromer in Parkinson's disease. *FEBS Lett* 2018;592(7):1096-1112.

25 Williams ET, Chen X, Otero PA, *et al*. Understanding the contributions of VPS35 and the retromer in neurodegenerative disease. *Neurobiol Dis* 2022;170:105768.

26 Morderer D, Wren MC, Liu F, *et al*. Probe-dependent proximity profiling (ProPPr) uncovers similarities and differences in phospho-tau-associated proteomes between tauopathies. *Mol Neurodegener* 2025;20(1):32.

27 Fan X, Xie Y, Cao S, *et al*. VPS35-retromer: multifunctional roles in various biological processes–a focus on neurodegenerative diseases and cancer. *J Inflamm Res* 2025;18:4665-4680.

28 Sassone J, Reale C, Dati G, *et al*. The role of VPS35 in the pathobiology of Parkinson's disease. *Cell Mol Neurobiol* 2021;41(2):199-227.

29 Li JG, Chiu J, Praticò D. Retraction Note to: Full recovery of the Alzheimer's disease phenotype by gain of function of vacuolar protein sorting 35. *Mol Psychiatry* 2023;28(2):965.

30 Morabito MV, Berman DE, Schneider RT, *et al*. Hyperleucinemia causes hippocampal retromer deficiency linking diabetes to Alzheimer's disease. *Neurobiol Dis* 2014;65:188-192.

31 Liu W, Tang FL, Erion J, *et al*. Vps35 haploinsufficiency results in degenerative-like deficit in mouse retinal ganglion neurons and impairment of optic nerve injury-induced gliosis. *Mol Brain* 2014;7(1):10.

32 Gao L, Xiao H, Ai LQ, *et al*. Vps35 deficiency impairs Cdk5/p35 degradation and promotes the hyperphosphorylation of tau protein in retinal ganglion cells. *Invest Ophthalmol Vis Sci* 2020;61(1):1.

33 Sorrentino FS, Allkabes M, Salsini G, *et al*. The importance of glial cells in the homeostasis of the retinal microenvironment and their pivotal role in the course of diabetic retinopathy. *Life Sci* 2016;162:54-59.

34 Güler BE, Krzysko J, Wolfrum U. Isolation and culturing of primary mouse astrocytes for the analysis of focal adhesion dynamics. *STAR Protoc* 2021;2(4):100954.

35 Dorrell MI, Aguilar E, Jacobson R, *et al*. Maintaining retinal astrocytes normalizes revascularization and prevents vascular pathology associated with oxygen-induced retinopathy. *Glia* 2010;58(1):43-54.

36 ValdezGuerrero AS, Quintana-Pérez JC, Arellano-Mendoza MG, *et al*. Diabetic retinopathy: important biochemical alterations and the main treatment strategies. *Can J Diabetes* 2021;45(6):504-511.

37 Tam J, Dhamdhere KP, Tiruveedhula P, *et al*. Subclinical capillary changes in non-proliferative diabetic retinopathy. *Optom Vis Sci* 2012;89(5):E692-703.

38 Verma A, Rani PK, Raman R, *et al*. Is neuronal dysfunction an early sign of diabetic retinopathy? Microperimetry and spectral domain optical coherence tomography (SD-OCT) study in individuals with diabetes, but no diabetic retinopathy. *Eye (Lond)* 2009;23(9):1824-1830.

39 Kern TS, Barber AJ. Retinal ganglion cells in diabetes. *J Physiol* 2008;586(18):4401-4408.

40 Hawkins BT, Davis TP. The blood-brain barrier/neurovascular unit in health and disease. *Pharmacol Rev* 2005;57(2):173-185.

41 Sofroniew MV, Vinters HV. Astrocytes: biology and pathology. *Acta Neuropathol* 2010;119(1):7-35.

42 Llorián-Salvador M, Cabeza-Fernández S, Gomez-Sanchez JA, *et al*. Glial cell alterations in diabetes-induced neurodegeneration. *Cell Mol Life Sci* 2024;81(1):47.

43 Fernandez DC, Pasquini LA, Dorfman D, *et al*. Early distal axonopathy of the visual pathway in experimental diabetes. *Am J Pathol* 2012;180(1):303-313.

44 Simó R, Hernández C. Neurodegeneration in the diabetic eye: new insights and therapeutic perspectives. *Trends Endocrinol Metab* 2014;25(1):23-33.

45 Liddelow SA, Marsh SE, Stevens B. Microglia and astrocytes in disease: dynamic Duo or partners in crime? *Trends Immunol* 2020;41(9):820-835.

46 Zhao Y, Lee D, Zhu XJ, *et al*. Critical role of neuronal Vps35 in blood vessel branching and maturation in developing mouse brain. *Biomedicines* 2022;10(7):1653.

47 Maloney MT, Wang X, Ghosh R, *et al*. LRRK2 kinase activity regulates Parkinson's disease-relevant lipids at the lysosome. *Mol Neurodegener* 2025;20(1):89.

48 Lange LM, Levine K, Fox SH, *et al*. The LRRK2 p.L1795F variant causes Parkinson's disease in the European population. *NPJ Parkinsons Dis* 2025;11(1):58.

49 Yang S, Xia C, Li S, *et al*. Mitochondrial dysfunction driven by the LRRK2-mediated pathway is associated with loss of Purkinje cells and motor coordination deficits in diabetic rat model. *Cell Death Dis* 2014;5(5):e1217.

50 Nguyen APT, Tsika E, Kelly K, *et al*. Dopaminergic neurodegeneration induced by Parkinson's disease-linked G2019S LRRK2 is dependent on kinase and GTPase activity. *Proc Natl Acad Sci U S A* 2020;117(29):17296-17307.

51 Mir R, Tonelli F, Lis P, *et al*. The Parkinson's disease VPS35 [D620N] mutation enhances LRRK2-mediated Rab protein phosphorylation in mouse and human. *Biochem J* 2018;475(11):1861-1883.

52 Linhart R, Wong SA, Cao J, *et al*. Vacuolar protein sorting 35 (Vps35) rescues locomotor deficits and shortened lifespan in Drosophila expressing a Parkinson's disease mutant of Leucine-rich repeat kinase 2 (LRRK2). *Mol Neurodegener* 2014;9(1):23.

53 Pajarillo E, Rizor A, Lee J, *et al*. The role of astrocytic glutamate transporters GLT-1 and GLAST in neurological disorders: Potential targets for neurotherapeutics. *Neuropharmacology* 2019;161:107559.

54 Murphy-Royal C, Dupuis JP, Varela JA, *et al*. Surface diffusion of

astrocytic glutamate transporters shapes synaptic transmission. *Nat Neurosci* 2015;18(2):219-226.

55 Malik AR, Willnow TE. Excitatory amino acid transporters in physiology and disorders of the central nervous system. *Int J Mol Sci* 2019;20(22):5671.

56 Iovino L, Giusti V, Pischedda F, *et al*. Trafficking of the glutamate transporter is impaired in LRRK2-related Parkinson's disease. *Acta Neuropathol* 2022;144(1):81-106.

57 Iovino L, Tremblay ME, Civiero L. Glutamate-induced excitotoxicity in Parkinson's disease: The role of glial cells. *J Pharmacol Sci* 2020;144(3):151-164.

58 Izquierdo-Altarejos P, Martínez-García M, Felipo V. Extracellular vesicles from hyperammonemic rats induce neuroinflammation in hippocampus and impair cognition in control rats. *Cell Mol Life Sci* 2023;80(4):90.

59 Aveleira CA, Lin CM, Abcouwer SF, *et al*. TNF-α signals through PKCζ/NF-κB to alter the tight junction complex and increase retinal endothelial cell permeability. *Diabetes* 2010;59(11):2872-2882.

60 Jiang N, Chen XL, Yang HW, *et al*. Effects of nuclear factor κB expression on retinal neovascularization and apoptosis in a diabetic retinopathy rat model. *Int J Ophthalmol* 2015;8(3):448-452.

61 Tang L, Zhang C, Yang Q, *et al*. Melatonin maintains inner blood-retinal barrier *via* inhibition of p38/TXNIP/NF-κB pathway in diabetic retinopathy. *J Cell Physiol* 2021;236(8):5848-5864.

62 Koksaldi S, Karti O, Saatci AO. Anti-vascular endothelial growth factor therapies in ophthalmology. *Med Hypothesis Discov Innov Ophthalmol* 2025;14(3):107-135.

63 Ramos H, Simó-Servat O. Neuroprotection in diabetes retinal disease: an unmet medical need. *Int J Mol Sci* 2026;27(2):901.

64 McCarron KR, Elcocks H, Mortiboys H, *et al*. The Parkinson's disease related mutant VPS35 (D620N) amplifies the LRRK2 response to endolysosomal stress. *Biochem J* 2024;481(4):265-278.

65 Mabrouk OS, Tichler B, Arnold HM, *et al*. LRRK2-targeting antisense oligonucleotide in Parkinson's disease: a phase 1 randomized controlled trial. *Nat Med* 2026;32(4):1421-1431.

66 Kamesh A, Kadgien CA, Kuhlmann N, *et al*. Emergent glutamate & dopamine dysfunction in VPS35(D620N) knock-in mice and rapid reversal by LRRK2 inhibition. *NPJ Parkinsons Dis* 2025;11:106.

67 Liu D, Zheng Z, Chen Z, *et al*. Ferroptosis in Müller cells under hyperglycemia: mechanisms and therapeutic implications for diabetic retinopathy-associated optic neuroinflammation. *Int Ophthalmol* 2025;45(1):302.

68 Li HY, Wang J, Xiao T, *et al*. STING immune activation of microglia aggravating neurovascular unit damage in diabetic retinopathy. *Free Radic Biol Med* 2025;233:86-101.